RU(II) sensitized Nb_2O_5 solar cell made by the sol-gel process

P. Guo, M.A. Aegerter*

Institute for New Materials - INM, Department of coating Technology, Im Stadtwald, Gebäude 43, D-66123 Saarbrücken, Germany

Abstract

Since the development of dye sensitized nanocrystalline TiO_2 solar cells by Grätzel et al., several other semiconducting electrode materials have been tested. The results obtained for solar cells of similar configuration using Nb_2O_5 layers are presented. 6μm thick Nb_2O_5 films have been deposited on conducting ITO or FTO glass by spin and dip coating process and sintered in air at 520°C. The layers are porous and crystalline with particle size ranging between 20 and 100 nm. Spectral sensitization of the films was carried out with a ruthenium(II)-complex, cis-Di(thiocyanato)-N,N′-bis(2,2′-bipyridyl-4,4′dicarboxylic acid)-ruthenium(II) dihydrate). The spectral incident photon to current conversion efficiency (IPCE) measured with a photoelectrochemical cell for a 4.9 cm^2 electrode has a maximum value of 40% at 520 nm. Closed solar cells of different sizes have been built and their photocurrent, open circuit voltage, fill factor and efficiency have been measured under tungsten halogen lamp irradiation up to 1000 W/m^2. The results obtained with a 0.2 cm^2 closed cell for a 100 W/m^2 (1/10 Sun) are $i_{sc} = 1.7$ mA/cm^2, $U_{oc} = 0.57$ V, $FF = 0.55$, $\eta = 5\%$. The conversion efficiency decreases with the light intensity. The influence of the Nb_2O_5 microstructure on the performance of the solar cell and a comparison with nanocrystalline TiO_2 solar cell are presented.

Keywords: Solar cells; Photoelectrochemical cells; Niobium oxide; Sol-gel process

1. Introduction

A new kind of solar cell based on dye sensitized nanocrystalline TiO_2 has been developed by Grätzel and coworkers[1–4]. It consists of a nanocrystalline thick film deposited on a transparent conducting glass substrate where the particles have been coated with a monolayer of a Ru(II)-complex adsorbed chemically, an electrolyte with an iodide/triiodide redox mediator and a counter electrode comprising a catalyst. The claimed overall conversion efficiency is 7–12% with an open circuit photovoltage of 0.72–0.83 V under 1000 W/m^2 sun simulator irradiation. Other large bandgap semiconducting electrodes have been tested as e.g. ZnO[5–8], SnO_2[9–14] and Nb_2O_5[15].

Nb_2O_5 is a semiconductor with a large band gap like TiO_2 (about 3.2 eV) but its conduction band lies at least 250 mV above that of TiO_2 [16]. It is expected that photoelectrochemical cells made with Nb_2O_5 exhibit a higher photovoltage. Photoelectrochemical studies in the UV-spectral region have shown that Nb_2O_5 sol-gel films present a photoelectric effect however smaller than that of TiO_2 films [17].

The paper presents the preparation and the photoelectrochemical performance of niobia Ru(II)-sensitized open and closed cells. The influence of the sol-gel made electrode microstructure on the solar cell efficiency and its photoelectrochemical response is reported and discussed.

2. Experimental

Nanocrystalline Nb_2O_5 sol-gel films were deposited on conducting glass substrate (ITO, 10 Ω (Asahi Glass) or FTO, 10 Ω (Donnelly)) by dip coating at a withdrawal rate of 0.5 mm/s and spin coating (1000 rev/min) using a partially hydrolyzed ethanolic Nb_2O_5 sol. The sol for dip coating deposition was prepared by dissolving $NbCl_5$ (Aldrich) in ethanol with a 0.32 mol Nb/l concentration. After addition of acetic acid and water, the sol was submitted to ultrasound during 5 min and then boiled with reflux for 2 h. For spin coating this sol was concentrated to 0.64 mol Nb/l by distillation of the solvent. After deposition, each layer was dried at room temperature and then heat treated at 400°C for 10 min, and the deposition process was repeated to increase the thickness of the coating. The last coating was sintered for 30 min in air at temperatures between 400 and 650°C. Dye sensitization was carried out by soaking the coatings for 30 h in a 1×10^{-3} mol/l ethanolic Ru(II)-solution synthesized following reference [2]. (Ru(II): cis-Di(thiocyanato)-N,N′-bis(2,2′-bipyridyl-4,4′-

* Corresponding author. Tel.: + 0049-681-9300317; fax: + 0049-681-9300249.

E-mail address: aegerter@inm-gmbh.de (M.A. Aegerter)

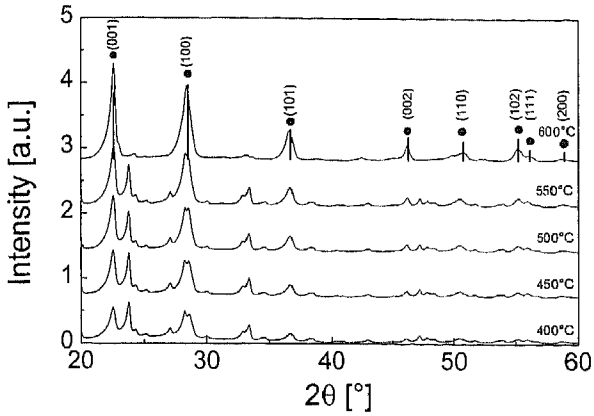

Fig. 1. X-ray pattern of spin coated Nb_2O_5 sol-gel films, sintered at different temperatures during 30 min. The position of X-ray peaks of JCPDS 28-317 is also shown (normalized to the height of the (100) peak).

dicarboxylic acid)-ruthenium(II) dihydrate, $(RuL_2(NCS)_2) \times 2H_2O$).

X-ray diffraction patterns of the films were measured with a Siemens Diffractometer D500. The morphology of the films was observed by scanning electron microscopy (SEM, JEOL JSM 6400 F) and their pore size distribution was determined using a Micromeritics ASAP 2400 N_2 adsorption-desorption equipment.

The single compartment photoelectrochemical cell consists of the dye-sensitized Nb_2O_5 photoelectrode (cell window), a Pt plate as counter electrode and a 0.01 M $Ag/AgClO_4$ as reference electrode. The electrolyte was prepared by dissolving 0.5 M $(Pr)_4NI$, 0.02 M LiI, and 0.04 M I_2 in a mixture of ethylene carbonate (48%), propylene carbonate (12%) and acetonitrile (40%). The closed devices were prepared as above, with a counter electrode manufactured by sputtering Pt onto an ITO conducting glass. The devices were sealed with a cyanacrylate glue.

The experimental set up for the IPCE measurements consisted of a 150 W tungsten halogen lamp, a monochromator (270M ISA Jobin Yvon–Spex), a beam splitter (LOT), a silicon photodiode (Hamamatsu) and a potentiostat (Bank Elektronik). The photocurrent-voltage characteristics were measured with an EG and G 273A potentiostat under irradiation with a 150 W tungsten halogen lamp. The irradiance was measured with a Radialux global sensor (Heraeus Instruments) in the spectral range 300–800 nm. The absorption spectrum of the Ru(II) solution was measured with a CARY 5E spectrophotometer.

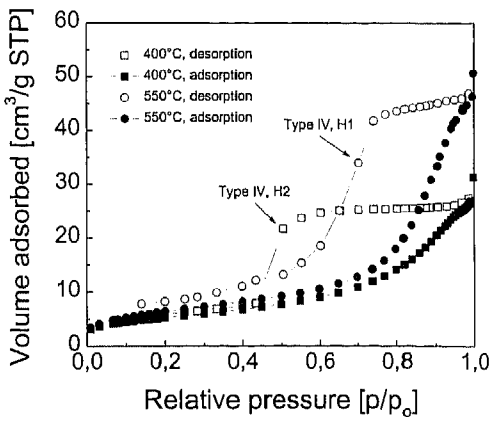

Fig. 2. N_2-adsorption and desorption isotherms of thick Nb_2O_5 coating sintered at 400 and 500°C temperatures. Solid symbols, adsorption; open symbols, desorption

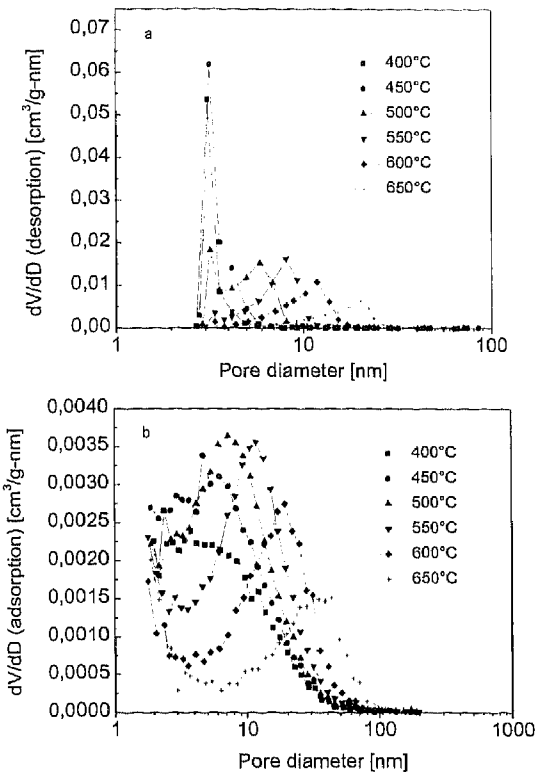

Fig. 3. Pore volume distribution dV/dD calculated from desorption data (a) and adsorption data (b) of Fig. 2.

3. Results and discussion

3.1. Coating structure and morphology

The X-ray diffraction pattern of multilayer spin coated Nb_2O_5 sol-gel film spun on borosilicate glass substrates and sintered at different temperatures during 30 min is shown in Fig. 1. The crystallization is observed at 400°C. Many peaks observed at low sintering temperatures get smaller or disappear at 600°C. The structure consists of different phases, one of them being the hexagonal phase (JCPDS No. 28-317). At 600°C only this phase is observed. The crystallites are partially oriented along the (001) direction. Their size increases from 13 to 19 nm ((001) peak) and from 32 to 41 nm ((100) peak) for samples heat treated at 400 and 600°C, respectively.

Fig. 2 shows typical N_2-adsorption and desorption

Table 1
Influence of the sintering temperature on BET surface area, BJH cumulative desorption pore volume of pore between 1.7 and 300 nm, micropore volume, BJH adsorption and desorption average pore diameters (4 V/A) of Nb_2O_5 films

Sintering temperature (°C)	400	450	500	520	550	600	650
BET surface area (m^2/g)	19 ± 0.1	25 ± 0.3	26 ± 0.2	25 ± 0.4	24 ± 0.2	17 ± 0.2	13 ± 0.1
BJH cumulative desorption pore volume of pores between 1.7 and 300 nm ($\times 10^{-2}$ cm^3/g)	4.3	5.3	6.3	6.9	7.3	7.5	7.4
Micropore volume ($\times 10^{-2}$ cm^3/g)	0.03	~0	0.07	~0	~0	~0	~0
BJH adsorption average pore diameter (4 V/A) (nm)	8.5	8.0	9.4	10.0	11.2	16.6	23.7
BJH desorption average pore diameter (4 V/A) (nm)	3.5	3.8	5.2	6.0	7.7	10.5	16.8

isotherms of thick Nb_2O_5 coating deposited on 0.4 mm AF45® (DESAG, Germany) glass substrates. Coatings sintered at 400°C show an adsorption isotherm of type IV with a hysteresis of type H2, typical of ink-bottle shaped mesopores. At higher sintering temperature the adsorption isotherm is also of type IV but the hysteresis tends to type H1, typical of cylindric pores. The pore size distribution of films sintered at different temperatures calculated from the desorption data which leads to values of the core diameters of the neck is shown in Fig. 3a and Table 1. At 400°C the BJH average pore diameter (4 V/A) is very small (3.5 nm) with a narrow distribution and the BJH cumulative volume of pores smaller than 300 nm is about 0.04 cm^3/g. With increasing sintering temperature the average pore diameter shifts steadily to higher value, the pore distribution increases and the BJH total pore volume slightly increases to ca. 0.075 cm^3/g, at 600°C. Fig. 3b and Table 1 show the pore size distribution determined from the adsorption isotherms which reflects the value of the core diameters of the body [18]. At all sintering temperatures the pore distributions are wider than those obtained from the desorption values. The average pore diameter also shifts towards larger values as the sintering temperature is increased. The comparison of the evolution of both distributions of average diameters (Table 1) confirms the presence of ink-bottle shaped pores which evolve into more cylindric pores as the temperature increases.

BET surface area of the coatings are also given in Table 1 for sintering temperatures ranging from 400 to 600°C. For all temperatures, the BET values are small and practically constant (~25 m^2/g) up to 550°C and then decrease.

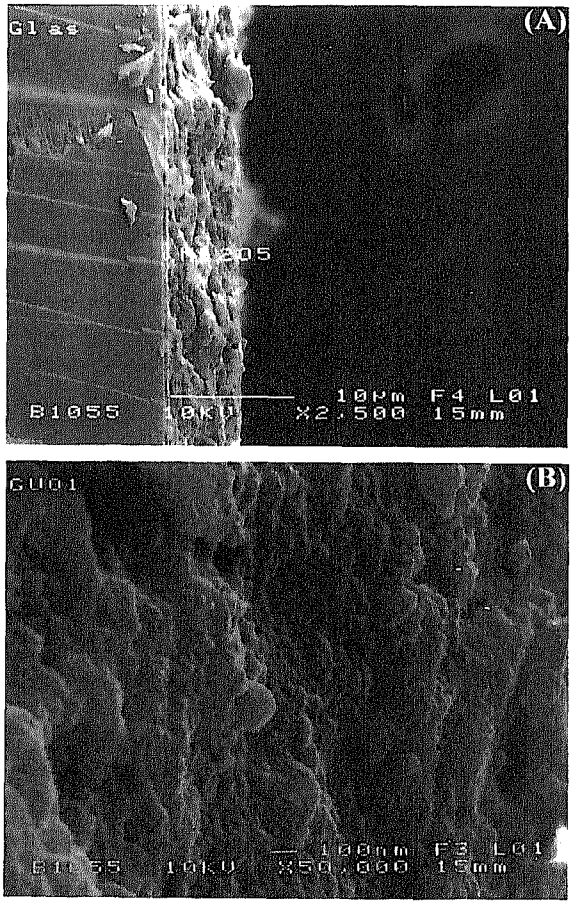

Fig. 4. SEM cross-section of a 6 µm thick Nb_2O_5 sol-gel film, sintered at 520°C for 30 min, deposited on conducting FTO glass substrate. (A), low resolution; (B), high resolution.

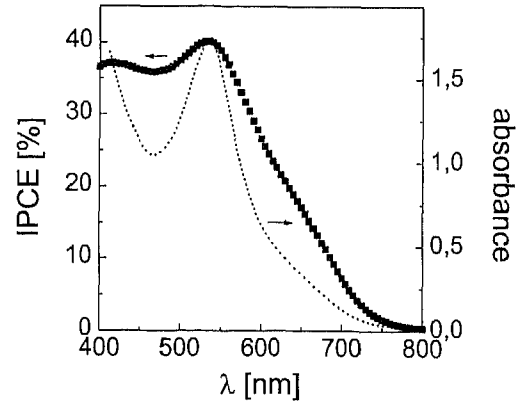

Fig. 5. Photocurrent action spectrum (■) of a 4.9 cm^2 Ru(II)-sensitized Nb_2O_5 photoelectrode and absorption spectrum (–) of $RuL_2(NCS)_2$ dye in ethanol solution.

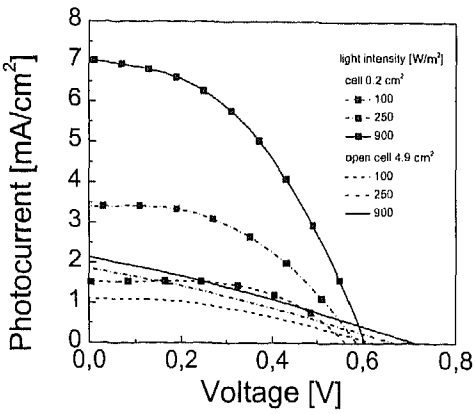

Fig. 6. Photocurrent-voltage characteristics of a 4.9 cm^2 Ru(II)-sensitized Nb_2O_5 open cell and a 0.2 cm^2 device under different illumination intensities.

Fig. 4 shows SEM cross-sections of a 6 μm thick coating sintered at 520°C with two different magnifications. The low resolution picture (A) shows the three-layer structure of the cell: glass substrate, FTO-layer and the 6 μm thick Nb_2O_5 film. The high resolution image (B) shows the 3-D morphology of the film made of Nb_2O_5 particles with size ranging between 20 and 100 nm.

3.2. Photoelectrochemical characteristics of open cells and devices

The incident monochromatic photon to current conversion efficiency (IPCE) of Ru(II) adsorbed on Nb_2O_5, defined as the ratio of the number of electrons generated by the light irradiation to the number of incident photons, is shown for a 4.9 cm^2 open cell in Fig. 5. The niobia coating was sintered at 520°C. The similarity between the absorption and action spectra suggests that the photosensitization mechanism is operative in the generation of the photocurrent i.e. photons absorbed by the dye molecules give rise to electrons injection into the conduction band of the semiconductor [1]. A maximum value of 40% is obtained under illumination from the substrate side. This is to be compared with a value of 85–90% obtained for optimized Ru(II)-sensitized TiO_2 electrode [2].

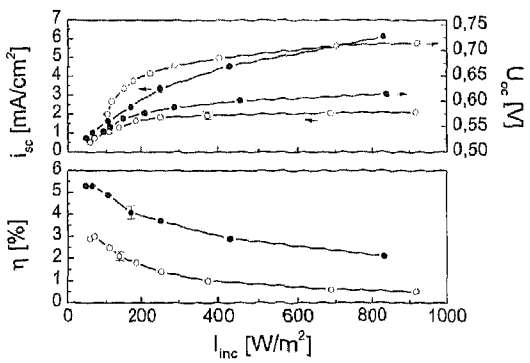

Fig. 7. Dependence of i_{sc}, U_{oc} and η with the illumination intensity for a 4.9 cm^2 open cell (O) and a 0.2cm^2 closed cell (●).

Fig. 6 shows the photocurrent-voltage curves obtained under different irradiation intensities for the 4.9 cm^2 Ru(II)-sensitized Nb_2O_5 open cell and a 0.2 cm^2 device prepared with a 6 μm thick Nb_2O_5 coating sintered at 520°C. The shapes of the *I–V* curves are different. For the 4.9 cm^2 open cell the short-circuit photocurrent i_{sc}, open-circuit voltage U_{oc}, fill factor *FF* and overall conversion efficiency η measured under 100 W/m^2 light irradiation are 1.09 mA/cm^2, 0.63 V, 0.39 and 2.5%, respectively. For the 0.2 cm^2 device the values are $i_{sc} = 1.6$ mA/cm^2, $U_{oc} = 0.57$ V, $FF = 0.56$ and $\eta = 5.0\%$ under the same light intensity. When the illumination intensity, I_{inc}, increases, the short-circuit photocurrent i_{sc} increases but exhibits a non-linear dependence on illumination intensity and saturates while the open-circuit photovoltage U_{oc} increases only slightly (Fig. 7). The overall conversion efficiency η decreases from 3.0 to 0.5% for the 4.9 cm^2 open cell and from 5.0 to 2.2% for the 0.2 cm^2 device. As expected the small area device shows a better efficiency than the large area cell but the value is still smaller than that reported for TiO_2. This is related to the low BET surface area of the electrode (about 25 m^2/g compared to ca. 100 m^2/g for TiO_2 (Table 2) which put a limit for the amount of Ru–complex adsorbed on the particles. A porous material with high surface area will increase the harvesting efficiency as more dye will be adsorbed on the electrode [19]. Therefore, in order to get higher value of i_{sc} and η at any illumination intensity it is necessary to find a way to increase the BET

Table 2
Comparison of different dye-sensitized solar cell

Photoelectrode	Area (cm^2)	Irradiance (W/m^2)	U_{oc} (V)	i_{sc} (mA/cm^2)	*FF*	η (%)	BET area (m^2/g)	Average pore size (nm)
TiO_2 [3]	0.4	1000	0.83	11.3	0.71	6.7	104 [19][b]	20 [19][b]
Nb_2O_5	0.2	900	0.61	7.0	0.44	2.2	25[a]	6[a]
		100	0.57	1.6	0.56	5		
TiO_2 [4]	9	1000	0.45	7–8	0.3–0.4	1.2		
Nb_2O_5	4.9	900	0.72	2.1	0.29	0.5		
		100	0.63	1.1	0.4	2.5		

[b] Sintered at 450°C, for 30 min.
[a] Sintered at 520°C, for 30 min.

values by at least a factor of three to four. The decrease of the conversion efficiency with the illumination intensity is essentially due to the non-linear increase and saturation of the current density. This probably reflects the fact that the pore size value (10 nm at 520°C (Table 1) compared to ca. 20 nm for TiO_2 (Table 2) and especially the pore neck diameters (6 nm at 520°C) are also too small and exhibit an ink-bottle shape. Under increasing light illumination intensity the I^- and I or I_3^- ions cannot diffuse fast enough in and out of the pores to regenerate the dye molecules. It is therefore also necessary to find a way to modify the pores structure and to increase their size. Works are presently underway to improve the morphology of the coatings.

A comparison of the results obtained with the Nb_2O_5 cells and those found in the literature for optimized TiO_2 cells of about the same dimensions is shown in Table 2. Due to their much higher values of BET area and average pore size, the small area device made of TiO_2 exhibit better value for all electrical parameters and this confirms that better characteristics should be obtained for Nb_2O_5 electrode if similar structure parameters can be obtained. A larger electrode area also degrades the electric and optical parameters of TiO_2 cells and the values obtained for Nb_2O_5 are quite similar.

4. Conclusions

Ru(II)-sensitized Nb_2O_5 film solar cells have been prepared by a sol-gel process using a niobium chloroalkoxide as precursor. Under low illumination intensity the overall solar to electric energy conversion efficiency is somewhat smaller than those obtained for cells made with nanocystalline TiO_2 particles. Moreover the efficiency of niobia solar cell diminishes (reversibly) with the increase of the illumination intensity. A comparison of the microstructure of Nb_2O_5 and TiO_2 electrodes shows that the lower photoelectrochemical performance of the Ru(II)-sensitized Nb_2O_5 solar cells is probably due to the lower BET surface area of the coatings that leads to a lower amount of dye adsorbed in the electrode and to the smaller average diameter of the pores. Their peculiar ink-bottle shape with narrow neck's diameter also limits the electrolyte mass transfer and slows down the dye regeneration.

Acknowledgements

Research financed by the 'Bundesministerium für Bildung und Forschung (BMBF) ' under contract 2A67/03N9040 and the state of Saarland (Germany).

References

[1] B. O'Regan, M. Grätzel, Nature 353 (1991) 737.
[2] M.K. Nazeeruddin, A. Kay, I. Rodicio, et al., J. Am. Chem. Soc. 115 (1993) 6382.
[3] A. Kay, M. Grätzel, Sol. Energy Mater. Sol. Cells 44 (1996) 99.
[4] O. Kohle, M. Grätzel, A.F. Meyer, T.B. Meyer, Adv. Mater. 9 (1997) 904.
[5] M. Spitler, M. Lübke, H. Gerisher, Ber. Bunsenges, Phys. Chem. 83 (1979) 663.
[6] T. Yamase, H. Gerisher, M. Lübke, Ber. Bunsenges, Phys. Chem. 83 (1979)) 658.
[7] W. Heiland, M. Bauer, Neuhaus, Photochem. Photobiol. 16 (1972) 315.
[8] I. Bedja, P.V. Kamat, X. Hua, A.G. Lappin, S. Hotchandani, Langmuir 13 (1997) 2398.
[9] A. Haraguchi, Y. Yonezawa, R. Hanawa, Photochem. Photobiol. 52 (1990) 307.
[10] M. Shimura, K. Shakushiro, Y. Shimura, J. Appl. Electrochem. 16 (1986) 683.
[11] H. Sato, M. Kawasaki, K. Kasatani, Y. Higuchi, T. Nishiyama, J. Phys. Chem. 92 (1988) 75.
[12] M. Krishnan, X. Zhang, A.J. Bard, J. Am. Chem. Soc. 106 (1984) 7371.
[13] I. Bedjia, S. Hotchandani, P.V. Kamat, J. Phys: Chem. 98 (1994) 4133.
[14] I. Bedjia, P.V. Kamat, S. Hotchandani, J. Appl. Phys 80 (1996) 4637.
[15] L. Hu, M. Wolf, M. Grätzel, Z. Jiang, J. Sol-Gel Sci, Technol. 5 (1995) 219.
[16] R. Vogel, H. Weller, SPIE 1729 (1992) 82.
[17] D.A. Barros, P. Filho, P. Abreu Filho, U. Werner, M.A. Aegerter, J. Sol-Gel Sci. Tech. 8 (1997) 735.
[18] S.J. Gregg, K.S.W. Sing, Adsorption, 2nd ed., Surface Area and Porosity, Academic Press, London, 1982.
[19] C.J. Barbe, F. Arende, P. Comte, M. Jirousek, F. Lenzmann, V. Shklover, M. Grätzel, J. Am. Ceram. Soc. 80 (1997) 3157.